Bulgarian Chemical Communications, Volume 49, Special Issue F, (pp. 100 - 106) 2017

Effect of the particle sizes on the thermoelectric efficiency of metal substituted $LaCo_{1-x}Ni_xFe_xO_3$ perovskites and $Zn_{1-x}Al_xO$ wurtzite

S.G. Harizanova[1*], E.N. Zhecheva[1], V.D. Valchev[2], M.G. Khristov, P.V. Markov[1], R.K. Stoyanova[1]

[1]*Institute of General and Inorganic Chemistry, Bulgarian Academy of Sciences, Acad. G. Bonchev Str., Bldg. 11, Sofia 1113, Bulgaria*
[2]*Faculty of Physics, University of Sofia, 1164 Sofia, Bulgaria*

Submitted on July 27, 2016; Revised on October 24, 2016

This contribution aims to assess the effect of the particle sizes on the thermoelectric efficiency of oxides. Two groups of oxides are studied: *p*-type semiconductor $LaCo_{1-x}Ni_xFe_xO_3$ with a perovskite structure and *n*-type semiconductor $Zn_{1-x}Al_xO$ with a wurtzite structure. The particle sizes are simply varied from 20 to 500 nm by increasing the annealing temperature from 400 to 900 °C. Structural and morphological characterizations are carried out by powder XRD, SEM and TEM analysis. The thermoelectric efficiency of oxides is determined by the dimensionless figure of merit, calculated from the independently measured Seebeck coefficient, electrical resistivity and thermal conductivity. The results show that the particle dimensions affect mainly the electrical conductivity, while Seebeck coefficient and thermal conductivity remain unchanged.

Keywords: Thermoelectric oxides; cobalt-based perovskites and ZnO.

INTRODUCTION

Thermoelectric oxide materials are nowadays considered as a key factor for clean energy production of the future since they are able to generate electric energy by using waste, geothermal or solar heat as an energy source [1,2]. Since the first report on thermoelectric efficiency of layered sodium cobalt oxides in 1997 till now, there is a challenging research competition aimed at defining the most suitable oxide composition and structure having simultaneously a high Seebeck coefficient, a high electrical conductivity and a low thermal conductivity [1-3]. As a result, several groups of compounds have been proposed: *p*-type conducting materials including Co-based perovskites and misfit $Ca_3Co_4O_9$ oxides, as well as *n*-type conducting materials comprising metal doped $Zn_{1-x}M_xO$ and $SrTiO_3$ [4]. The state-of-the-art research is mainly devoted to the enhancement of the thermoelectric efficiency of oxides by a single metal substitution or by a particle-size engineering [5,6].

Recently we have demonstrated that the multiple substitution for cobalt ions in the framework of the perovskite-type structure is an effective way to improve the thermoelectric performance of $LaCoO_3$-based ceramics [7-9]. The best thermoelectric efficiency is established for Ni, Fe-double substituted cobaltates $LaCo_{0.8}Ni_{0.1}Fe_{0.1}O_3$, which is an order of magnitude higher than that of $LaCoO_3$ at room temperature [7-9]. The improved performance is explained with a synergic effect of Ni and Fe ions substituted for Co ions to reduce effectively thermal conductivity of cobaltates [7-9]. The strategy for the metal substitution is also fruitful for improving thermoelectric properties of ZnO semiconductor [10-12]. It has been found that substitution of aliovalent Al^{3+} ions for Zn^{2+} in regular lattice sites yields $Zn_{1-x}Al_xO$ oxides ($0<x\leq0.005$) with improved thermoelectric efficiency which is a consequence of the decreased electrical and thermal resistivity [10-12].

This contribution aims to examine the effect of the particle sizes on the thermoelectric efficiency of metal substituted $LaCo_{0.8}Ni_{0.1}Fe_{0.1}O_3$ perovskites and wurtzite-type $Zn_{0.995}Al_{0.005}O$. These two oxide compositions are chosen due to their high thermoelectric efficiencies reported early [7,12]. Both $LaCo_{0.8}Ni_{0.1}Fe_{0.1}O_3$ and $Zn_{0.995}Al_{0.005}O$ oxides are prepared by thermal decomposition of homogeneous precursors such as freeze-dried $LaCo_{0.8}Ni_{0.1}Fe_{0.1}$ citrates and co-precipitated $Zn_{0.995}Al_{0.005}$ carbonate-hydroxides, respectively. The temperature of oxide formation is determined from TG and DTA analyses. The particle sizes are simply varied by increasing the annealing temperature. Structural and morphological characterizations are carried out by powder XRD, SEM and TEM analysis. The thermoelectric efficiency of the oxides is determined by the dimensionless figure of merit, calculated from the independently measured Seebeck coefficient (S), electrical resistivity (ρ) and thermal conductivity (λ).

* To whom all correspondence should be sent:
E-mail: sonya@svr.igic.bas.bg

EXPERIMENTAL

Perovskite $LaCo_{0.8}Ni_{0.1}Fe_{0.1}O_3$ is obtained from corresponding freeze-dried citrates following the procedure described elsewhere [7]. The thermal decomposition of the citrate-precursors was achieved at 400ºC for 3 h in air. The obtained solid residue was annealed at 600 and 900 ºC for 40 h in air, then cooled down to room temperature with a rate of 5º/min.

Wurtzite-type oxide $Zn_{0.995}Al_{0.005}O$ is prepared by co-precipitation from aqueous solution of $Zn(NO_3)_2.6H_2O$ and $Al(NO_3)_3.9H_2O$ with NH_4HCO_3. The details are given in details elsewhere [12]. The mixed hydroxide-carbonate precipitates are treated at 450 and 700 ºC for 10h.

X-ray structural analysis is performed on a Brucker Advance 8 diffractometer with Cu Kα radiation. Step-scan recording for structure refinement is carried out using 0.02 º2θ steps of 5s duration. XRD patterns are analyzed by a structural model comprising rhombohedrally distorted perovskite-type structure (*R-3c* space group), as well as a model on the basis of wurtzite-type structure ($P6_3mc$ space group). The crystallite size of oxides was calculated by the Scherrer equation from the line width of the (012) and (024) perovskite reflection peaks, as well as of the (101) wurtzite peak: $D_{hkl} = \lambda / ((\beta^2 - \beta^2_o)^{1/2} \cos\theta_{hkl})$ where λ is CuKα radiation, β is the peak width at the half height corrected with instrumental broadening and θ_{hkl} is the Bragg angle. The line width was determined by profile analysis using a WinPlotr program.

SEM images of pellets coated with gold are obtained by Zeiss DSM 962 microscope and Philips XL30 scanning electron microscope. The TEM investigations are performed by TEM JEOL 2100 at accelerating voltage of 200 kV. The specimens are prepared by grinding and dispersing them in ethanol by ultrasonic treatment for 6 minutes. The suspensions are dripped on standard holey carbon/Cu grids. The analysis was carried out by the Digital Micrograph software.

The thermal analysis (simultaneously obtained DTA, TG and DTG) of precursors is carried out by a combined LABSYS^{TM} EVO DTA/TG system of the SETARAM Company, France, with a gas-analyser of the OmniStar™ type. The samples are investigated in air, a heating rate of 5 °C/min and sample mass of 10 mg.

The transport properties of the oxides are measured on pellets sintered at 600 and 900 ºC for 40 hours. Pellet density was determined by Archimedes' method. The property was evaluated by comparison with the theoretical density of $LaCoO_3$ and ZnO.

Electrical resistivity (ρ), density and mobility of charge carriers were determined by MMR's Variable temperatures Hall System (k2500-5SLP-SP) using Van der Pauw method over a temperature range of 250 - 600 K. The benchtop permanent magnet (0.5T) is used. Thermal conductivity was determined at room temperatures on Thermal Conductivity Analyzer TCi (SETARAM). In order to compare the thermal conductivities of samples having different porosity, the thermal conductivity is normalized to 95% of the theoretical density (λ_t) using the following density correction [13]: $\lambda_t = \lambda(0.95^{1.5})/(1-P)^{1.5}$, where λ is the measured thermal conductivity and P is the fractional porosity of the pellet.

RESULTS AND DISSCUSIONS

Structure and morphology of $LaCo_{0.8}Ni_{0.1}Fe_{0.1}O_3$ and $Zn_{0.995}Al_{0.005}O$

The organic component has been shown to be an important factor determining the thermal properties of precursors [14,15]. Figure 1 compares the DTA, DTG and TG curves of freeze-dried $LaCo_{0.8}Fe_{0.1}Ni_{0.1}$ citrate and co-precipitated $Zn_{0.995}Al_{0.005}$ carbonate-hydroxide. For citrates, the DTA curves display two endothermic processes at 149 and 180ºC, followed by strong exothermic process above 280 ºC (Fig. 1a). According to the thermal properties of citrate complexes [14-16], the endothermic processes can be assigned to the dehydration and to the transformation of the citrate into aconitate, while the exothermic processes correspond to the combustion of the residual organics. The process is finished at around 380ºC. The thermal decomposition of co-precipitated $Zn_{0.995}Al_{0.005}$ carbonate-hydroxide is accomplished at one endothermic peak at 246 ºC, the process being completed up to 300 ºC.

At 400 ºC and short heating time of 3 hours, the product of thermal decomposition of freeze-dried citrate is a mixture of cobalt-based perovskite, spinel and $La_2O_2CO_3$, which agree with our previous data [12,13]. The well-crystallized single perovskite phase is only obtained by increasing the temperature from 400 to 600 ºC, as well as by prolonging the heating time to 20 hours (Fig. 2). At these conditions, the XRD pattern consists only of rhombohedrally distorted perovskite phase $LaCo_{0.8}Fe_{0.1}Ni_{0.1}O_3$.

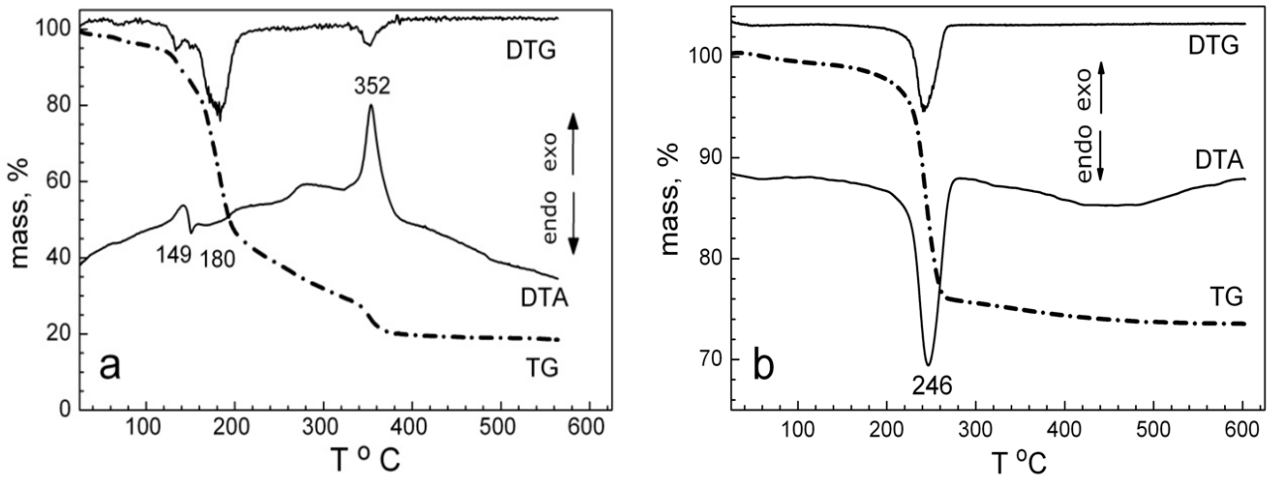

Figure 1. DTA, DTG and TG curves of freeze-dried $LaCo_{0.8}Fe_{0.1}Ni_{0.1}$ citrate (a) and co-precipitated $Zn_{0.995}Al_{0.005}$ carbonate-hydroxide (b).

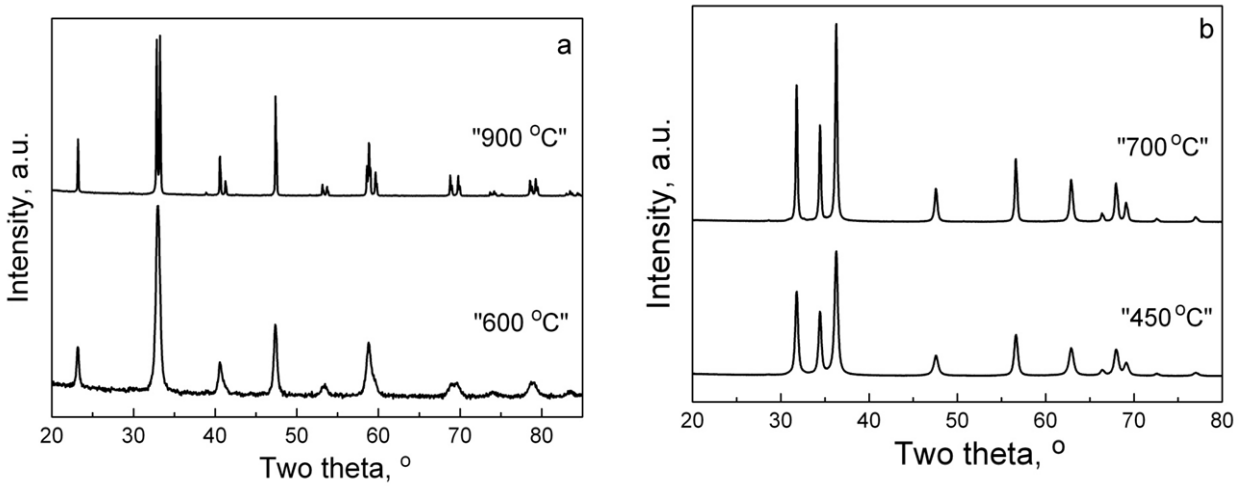

Figure 2. XRD patterns of $LaCo_{0.8}Ni_{0.1}Fe_{0.1}O_3$ (a) and $Zn_{0.995}Al_{0.005}O$ (b). The samples are annealed at 600 and 900°C for $LaCo_{0.8}Ni_{0.1}Fe_{0.1}O_3$, as well as at 450 and 700 °C for $Zn_{0.995}Al_{0.005}O$.

Table 1 Lattice parameters (*a*, *c*, *V*) and XRD crystallite sizes (r_{XRD}) for $LaCo_{0.8}Ni_{0.1}Fe_{0.1}O_3$ and $Zn_{0.995}Al_{0.005}O$.

Samples	Unit cell parameters			r_{XRD}, nm
	a±0.0001, Å	*c*±0.0003, Å	*V*, Å^3	
$LaCo_{0.8}Ni_{0.1}Fe_{0.1}O_3$-600	5.4470	13.1752	338.54	37
$LaCo_{0.8}Ni_{0.1}Fe_{0.1}O_3$-900	5.4532	13.1191	337.86	131
$Zn_{0.995}Al_{0.005}O$-450	3.2505	5.2084	47.66	22
$Zn_{0.995}Al_{0.005}O$-700	3.2504	5.2062	47.64	36

This means that the multiple substitutions at Co sites proceed in the framework of the perovskite type structure. Further annealing of $LaCo_{0.8}Fe_{0.1}Ni_{0.1}O_3$ at 900 °C does not provoke any changes in the perovskite structure. Lattice parameters for $LaCo_{0.8}Fe_{0.1}Ni_{0.1}O_3$ annealed at 600 and 900 °C are listed on Table 1. The only parameter that is changed is the line width of the diffraction peaks. Using the correlation between the line width and the crystal size, Table 1 gives also the calculated crystallite sizes for the perovskite annealed at low and high-temperature. The result reveals a strong increase in the XRD crystallite sizes (more than 3 times) when going from 600 to 900 °C.

The same picture is observed for Al doped ZnO. The well-crystalline wurtzite-type oxide is formed at 400 °C. The lattice parameters are close to that of

undoped ZnO: a = 3.2486 and c = 5.2035 [12]. Further annealing at 700 °C is related with an increase in the crystallite size of $Zn_{0.995}Al_{0.005}O$ without changing the lattice parameters (Table 1). The comparison shows that changes in the crystallite sizes are more restricted for $Zn_{0.995}Al_{0.005}O$ in comparison with that for the perovskite phase. Based on solid state ^{27}Al MAS NMR, we have established that aliovalent Al^{3+} ions substitute for Zn^{2+} in the wurtzite-type of structure when the samples are annealed in the temperature range of 400-700 °C [12]. As a result, the temperature range of annealing of Al-doped ZnO is chosen between 400 and 700 °C so that to ensure both the particle growth and the preservation of Al^{3+} ions inside the wurtzite structure. All XRD results reveal clearly that the perovskite and the wurtzite structures remain unchanged in the temperature range of annealing.

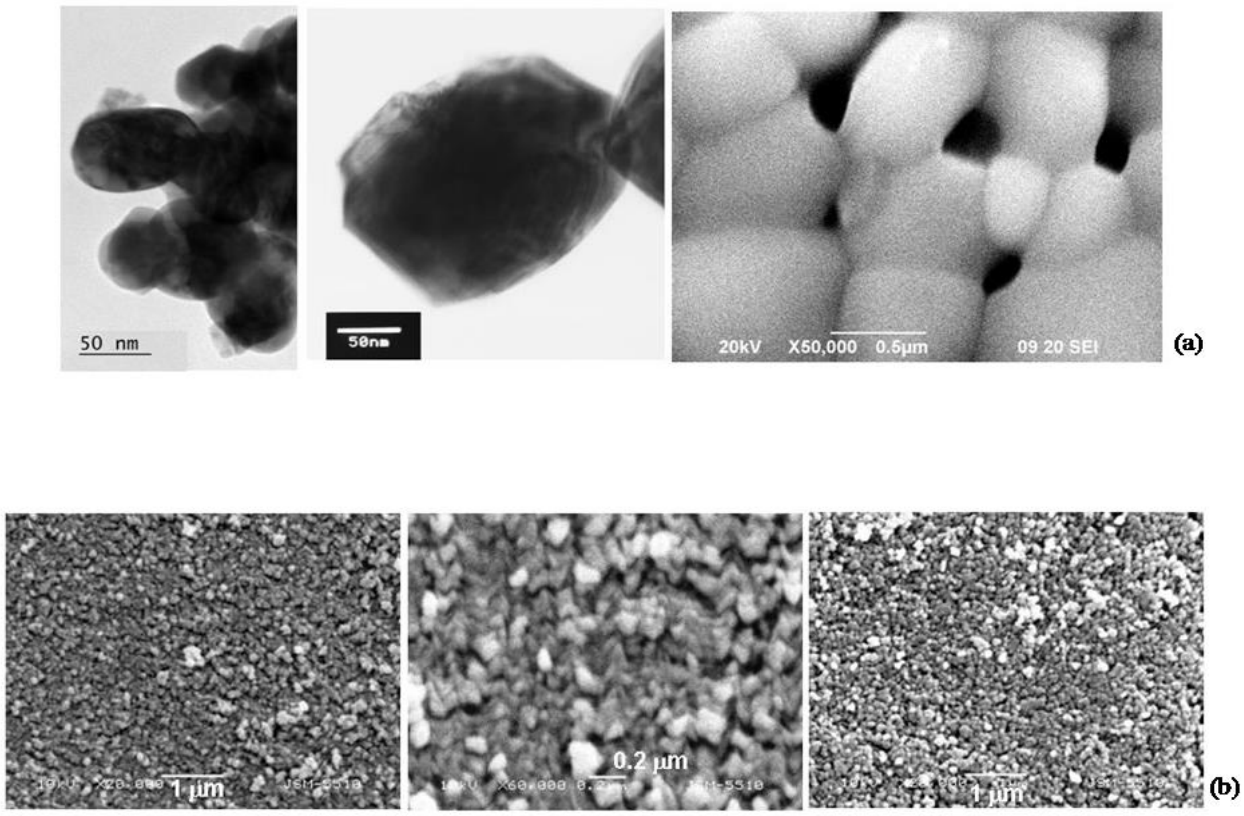

Figure 3. TEM and SEM images for $LaCo_{0.8}Ni_{0.1}Fe_{0.1}O_3$ (a) annealed at 600 and 900 °C. SEM images of $Zn_{0.995}Al_{0.005}O$ (b) annealed at 450 and 700 °C.

The morphology of the oxides is a critical parameter in order to fabricate the dense pellets suitable for electrical resistivity measurements. Therefore, Figure 3 compares the morphologies of $LaCo_{0.8}Ni_{0.1}Fe_{0.1}O_3$ and $Zn_{0.995}Al_{0.005}O$ having different particle dimensions. At low annealing temperature, $LaCo_{0.8}Ni_{0.1}Fe_{0.1}O_3$ displays well-shaped individual particles with a mean dimension of about 50 nm, while a significant crystal growth is observed at high annealing temperature: a mean particle size reaches a value of about 500 nm. The observed changes in the particle sizes during perovskite annealing are consistent with that established for the crystallite sizes calculated from XRD line width (Table 1). The temperature-induced changes in the morphology are less obvious for $Zn_{0.995}Al_{0.005}O$ (Fig. 3b), which is also in agreement with the calculated XRD crystallite sizes.

The important finding is the fact that both $LaCo_{0.8}Ni_{0.1}Fe_{0.1}O_3$ and $Zn_{0.995}Al_{0.005}O$ form dense pellets irrespective of the different particle dimensions. For the perovskite phase, well shaped particles fused one to another give rise to the pellet porosity varying between 20 – 25 %. Irrespective of the smaller particle sizes, the pellet porosity of

$Zn_{0.995}Al_{0.005}O$ is also close to 25 %. The similar pellet porosities allow us to compare the thermoelectric properties of samples having different particle dimensions.

Size-dependent transport properties of $LaCo_{0.8}Ni_{0.1}Fe_{0.1}O_3$ and $Zn_{0.995}Al_{0.005}O$

The performance of thermoelectric materials is usually characterized by the dimensionless figure of merit $ZT=S^2T/(\rho.\lambda)$ where S is the Seebeck coefficient, T is the absolute temperature, ρ is the electrical resistivity, and λ is the thermal conductivity. The improvement of their properties can be achieved by rational control of carrier density, electrical and thermal transport. All results on transport properties of the perovskite and the wurtzite phases are summarized on Figure 4 and Table 2.

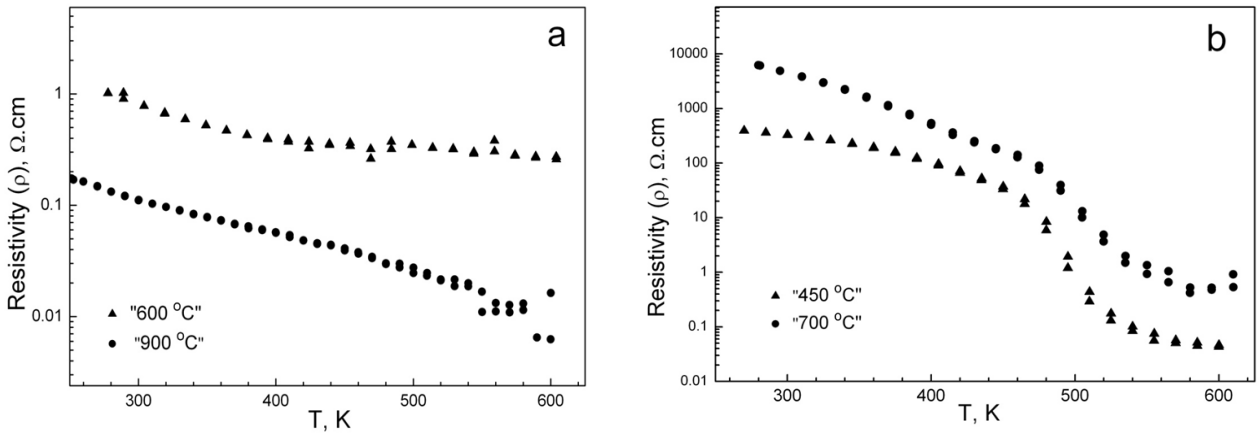

Figure 4. Temperature dependence of the electrical resistivity for $LaCo_{0.8}Ni_{0.1}Fe_{0.1}O_3$ (a) annealed at 600 and 900 °C, as well as for $Zn_{0.995}Al_{0.005}O$ (b) annealed at 450 and 700 °C.

Table 2. Electrical resistivity, carrier density (CD), carrier mobility (CM), Seebeck coefficient, thermal conductivity, power factor and figure of merit for $LaCo_{0.8}Ni_{0.1}Fe_{0.1}O_3$ annealed at 600 and 900 °C (P600, P900) and for $Zn_{0.995}Al_{0.005}O$ annealed at 450 and 700 °C, (W450, W700) respectively.

Samples	ρ, Ω.cm	CD, cm^{-3} x10^{18}	CM, cm^2/Vs	S, μV/K	λ, W/(m.K) ± 0.04	*PF*	*FM*
P600	0.793	2.9	2.5	+ 189	0.20	0.045	0.007
P900	0.072	8.6	2.7	+ 234	0.17	0.758	0.134
W450	333.5	1.5	0.01	- 259	0.33	2.0 x 10^{-4}	1.8 x 10^{-5}
W700	4570.1	0.05	0.03	-590	0.30	0.8 x 10^{-4}	0.8 x 10^{-5}

Figure 4 shows the temperature dependence of the electrical resistivity of $LaCo_{0.8}Ni_{0.1}Fe_{0.1}O_3$ and $Zn_{0.995}Al_{0.005}O$ having different particle dimensions. For all of the samples studied, the electrical resistivity decreases with raising the temperature from 250 to 600 K, thus indicating their semiconducting behaviour. While the electrical resistivity of the perovskite phase increases with decreasing the particle dimensions, the wurtzite phase displays an opposite trend: the electrical resistivity is higher for the sample having higher particle dimensions. It is worth mentioning that the changes in the resistivity of the wurtzite phase are more significant in comparison with that for the perovskite phase.

In accordance with our previous data, the temperature dependence of the electrical resistivity of $LaCo_{0.8}Ni_{0.1}Fe_{0.1}O_3$ annealed at 900 °C is describes by the model based on the nearest neighbors hopping of small polarons [$\rho=\rho_o Texp(-E_p/kT)$], the activation energy being 0.0909(5) eV [5]. It is noticeable that the same model can be used to describe most adequately the temperature dependence of the electrical resistivity of $LaCo_{0.8}Ni_{0.1}Fe_{0.1}O_3$ having one order smaller particle dimensions. Moreover, the activation energy for $LaCo_{0.8}Ni_{0.1}Fe_{0.1}O_3$ with smaller particles tends to that for $LaCo_{0.8}Ni_{0.1}Fe_{0.1}O_3$ with bigger particles: 0.093 eV. Contrary to the perovskite phase, the temperature dependence of the electrical resistivity for the wurtzite phase can not be described with one model in the temperature range of 250 – 600 K.

The observed changes in the resistivity for the perovskite and the wurtzite phases are related with the density and mobility of the charge carriers (Table 2). As one can see, for the perovskite phase the carrier density increases with an increase in the particle dimensions, while the carrier mobility remains the same. This means that the smaller the particle sizes, the lower the carrier density is. The observed dependence suggests that defects in the perovskite structure induced by the smaller particle

sizes destroy the charge carriers. Keeping the carrier mobility unchanged, the mechanism of the electrical conductivity stays insensitive towards the particle dimensions.

The wurtzite phase displays the opposite behavior. By increasing the particle dimensions, the charge carriers decrease. As in the case of the perovskite phase, the carrier mobility is insensitive towards the particle sizes. This indicates that size-induced defects in the wurtzite structure give rise to the charge carrier (Table 2).

The Seebeck coefficient is strongly dependent on the structure type (Fig. 8). All perovskites display positive sign of the Seebeck coefficient (*S*), thus indicating that the predominant mobile charge carriers are holes (*p*-type semiconductor). Contrary, the sign of the Seebeck coefficient is negative for the wurtzite phase, thus revealing that the predominant mobile charge carriers are electrons (*n*-type semiconductor). While the Seebeck coefficient remains size-independent for the perovskite phase, the wurtzite phase displays an increase in the Seebeck coefficient with particle dimensions.

The thermal conductivity is the next parameter that is independently determined for the perovskite and the wurtzite phases (Table 2). The results show that thermal conductivity does not undergo any measurable changes with variation of the particle sizes. This can be understood if we take into account the physical meaning of thermal conductivity. The thermal conductivity can be expressed by two terms due to the electronic and lattice contributions. For the oxides, the total the thermal conductivity is mainly governed by the lattice contribution. This means that the phonon scattering for the perovskite and the wurtzite structure is size-independent. The lattice contribution can be tentatively related with the carrier mobility, which is also size-independent parameter.

Taking into account the Seebeck coefficient and electrical resistivity data, the power factor is calculated: $PF=S^2/\rho$ (Table 2). In general, the comparison shows that *PF* is higher for the perovskite phase than the wurtzite phase. In addition, the highest *PF* is observed for the perovskite with bigger particle sizes. Contrary, the wurtzite phase with smaller particle sizes displays a high *PF* value.

In addition to *PF*, Table 2 gives also a calculated figure of merit. It appears that the perovskite phase with bigger particle sizes exhibits a highest thermopower activity, while the wurtzite phase with smaller particles has a better performance. This reveals that by a variation of the particle sizes it is possible to control the thermopower efficiency of the perovskite and the wurtzite phases in respect to their desired applications.

CONCLUSIONS

Two groups of compounds are studied in order to assess the effect of the particle dimensions on the thermoelectric efficiency: *p*-type semiconductor $LaCo_{0.8}Ni_{0.1}Fe_{0.1}O_3$ with a perovskite structure and *n*-type semiconductor $Zn_{0.995}Al_{0.005}O$ with a wurtzite structure. Although the bigger particles contribute to an increase in the thermopower activity of the perovskite phase, the wurtzite phase is better performed in the case when smaller particles dominate. The particle sizes affect mainly the density of charge carriers, while the carrier mobility, Seebeck coefficient and thermal conductivity are size-independents. The variation in the particle sizes has an opposite effect on the transport properties of the oxides in comparison with that of metal substitution: the metal additives reduce effectively the heat transport in the oxide matrices. This study demonstrates the capability to control the thermoelectric efficiency of oxides by rational combining of the type of crystal structure, the kind of metal dopants and sizes of the crystal particles.

Acknowledgment: *Authors are grateful to the financial support from ESF (Grant BG051PO001-3.3.06-0050).*

REFERENCES

1. S. Hébert, D. Berthebaud, R. Daou, Y. Bréard, D. Pelloquin, E. Guilmeau, F. Gascoin, O. Lebedev, A. Maignan *J. Phys. Condensed Matter* **28** (1), (2015) art. no. 013001.
2. J. W. Fergus, *J. Europ. Ceram. Soc.*, **32,** 3, 525 (2012).
3. I. Terasaki, Y. Sasago and K. Uchinokura, *Phys. Rev. B*, **56,** 12685 (1997).
4. S. Hébert, W. Kobayashi, H. Muguerra, Y. Bréard, N. Ragavendra, F. Gascoin, E. Guilmeau and A. Maignan, *Phys. Status Solidi A*, **210,** 69 (2013).
5. R. Robert, L. Bocher, M. Trottmann, A. Reller, A. Weidenkaff, *J. of Solid State Chem.*, **179**, 3893 (2006).
6. B. T. Geraldine, C. Dewei, X. Xinrun, Li. Sean, *Current Phys. Chem.*, **4**, 256 (2014).
7. V. Vulchev, L. Vassilev, S. Harizanova, M. Khristov, E. Zhecheva, R. Stoyanova, *J. Phys. Chem. C*, **116,** 13507 (2012).
8. S. Harizanova, E. Zhecheva, V. Valchev, M. Khristov, R. Stoyanova, *Materials Today: Proceedings 2*, 4256 (2015).
9. S. Harizanova, E. Zhecheva, M. Khristov, V. Valchev, R. Stoyanova, *Bulg. Chem. Commun.*, **48,** 82 (2016).

10. Z. L. Wang, *J. Phys.: Condens. Matter*, **16,** R829 (2004).
11. T. Tsubota, M. Ohtaki, K. Eguchi, H.Arai, *J. Mater. Chem.*, **7**, 85 (1997).
12. S. Harizanova, E. Zhecheva, R. Stoyanova, V. Valchev and M. Khristov, *Materials and Technologies for Energy Efficiency*, (ISBN-10: 1-62734-559-0; ISBN-13: 978-1-62734-559-0), Publisher: BrownWalker Press, Editor: A. Méndez-Vilas, 475 (2015).
13. B. Schulz, *High Temp. High Press*. **13,** 649 (1981).
14. S. Ivanova, A. Senyshyn, E. Zhecheva, K. Tenchev, V. Nikolov, R. Stoyanova, H. Fuess, *J. Alloys and Comp.* **480**, 279 (2009).
15. S. Ivanova, A.Senyshyn, E.Zhecheva, K.Tenchev, R.Stoyanova, H. Fuess, *J. of Solid State Chem.*, **183**, 940 (2010).
16. M. M. Milanova, M. G. Arnaudov, M. M. Getsova, D. S. Todorovsky, *J. of Alloys and Comp.*, **264,** 95 (1998).

ЕФЕКТ НА РАЗМЕРА НА ЧАСТИЦИТЕ ВЪРХУ ТЕРМОЕЛЕКТРИЧНАТА ЕФЕКТИВНОСТ НА МЕТАЛ ЗАМЕСТЕНИ $LaCo_{1-x}Ni_xFe_xO_3$ ПЕРОВСКИТИ И ВЮРЦИТ $Zn_{1-x}Al_xO$

С. Г. Харизанова[1*], Е. Н. Жечева[1], В. Д. Вълчев[2], М. Г. Христов[1], П. В. Марков[1], Р. К. Стоянова[1]

[1]*Институт по обща и неорганична химия, Българска академия на науките, бул. Акад. Г. Бончев, бл. 11, София 1113, България*
[2]*Физически Факултет,Софийски Университет, 1164 София, България*

Постъпила на 27 юли, 2016 г. коригирана на 24 октомври, 2016 г.

(Резюме)

Проведеното изследване има за цел да оцени ефекта на размера на частиците върху термоелектричната ефективност на оксидни материали. Два класа от оксиди са изследвани: полупроводници от *p*-тип $LaCo_{1-x}Ni_xFe_xO_3$ с перовскитова структура и полупроводници от *n*-тип $Zn_{1-x}Al_xO$ с вюртцитна структура. Размера на частиците са варирани от 20 до 500 nm чрез увеличаване на температурата на отгряване в интервала 400 – 900 ^oC. Структурното и морфологично охарактеризиране е проведено с използване на прахов рентгеново дифракционен анализ, SEM и TEM анализи. Термоелектричната ефективност е определена чрез безразмерната величина пресметната от независимо измерените коефициент на Зеебек, електрично съпротивление и термична проводимост. Резултатите показват, че размерът на частиците влияе основно върху електричната проводимост, докато коефициентът на Зеебек и термичната проводимост остават практически непроменени.